

Modern Building Materials, Structures and Techniques, MBMST 2016

Analytical modelling of combined slip and sliding modes in contact interaction of two spherical grains

Robertas Balevičius^{a*}, Zenon Mróz^b

^a*Department of Reinforced and Masonry Structures, Faculty of Civil Engineering, Vilnius Gediminas Technical University, Sauletekio av. 11, LT-10223 Vilnius, Lithuania*

^b*Department of Mechanics of Materials, Institute of Fundamental Technological Research, Polish Academy of Sciences, st. Pawińskiego 5b, 02-106 Warsaw, Poland*

Abstract

The analytical modelling of coupled slip and sliding contact response of two elastic spheres is presented for the kinematically imposed sphere centre relative motion trajectories. One sphere is assumed as a fixed, the other translating along a specified trajectory and remaining in contact condition. Two cases are considered, the first is corresponding to a linear trajectory with the contact engagement in the combined slip-sliding mode, the other is related to the contact initiation by normal loading and subsequent motion along an inclined linear trajectory. The formulae and diagrams of the evolution of driving force along the sliding path in terms of main contact geometry parameters were analytically specified. Further extensions and applications of the analysis can be envisaged in the creation of the translation controlled apparatus for the measurements of friction and restitution coefficients for the pair of spherical grains.

© 2017 Published by Elsevier Ltd. This is an open access article under the CC BY-NC-ND license (<http://creativecommons.org/licenses/by-nc-nd/4.0/>).

Peer-review under responsibility of the organizing committee of MBMST 2016

Keywords: soil, spherical grains contact interaction; slip and finite sliding modes; monotonic or reciprocal sliding; coefficients of friction and restitution.

* Corresponding author.

E-mail address: ^arobertas.balevicius@vgtu.lt; ^bzmroz@ippt.gov.pl

1. Introduction

The mechanical response of soils, fluidized beds, is mainly predicted in the framework of continuum mechanics and rules of the theories of elasticity and plasticity. Such approach allows for establishing the main bulk parameters without any consideration of the behavior of individual grains at their micro scale and the effects arising in microstructure of granules during the transient flow. Alternatively, the same bulk properties of granular matter can be determined using the homogenization approach, when the micro-level contact interaction parameters are defined. In this case, the micro-level based parameters, such as, the normal and tangential compliances, contact stiffness, friction coefficient, adhesive strength or viscosity modulus established from the grain-grain contact mechanics are required. As a rule, the micro-mechanical approach requires the numerical analysis [1], [2].

The pioneering analysis of two spheres contact interaction under the applied normal to contact plane forces was developed by Hertz. For the sphere-sphere contact interaction, when normal and tangential forces are applied, the theory has been developed by Mindlin and Deresiewicz [3]. However, this theory is suitable for very small tangential displacement ranges, operating in a so called slip mode, and is not appropriate, when the contact zone is no longer fixed and sliding of the sphere occurs. For a specified trajectory of the sphere center, both normal and tangential forces vary and the contact zone changes its size and orientation, cf. [4], [5].

The present paper is aimed at developing the analytical description of interaction of two contacting spheres for several classes of combined slip and sliding trajectories, typical in the experimental testing. In particular, one sphere is being fixed, the other allowed to execute a translatory motion with the constraint set on its rotation. The case, when the contact zone is first generated by applying the normal load and next a combined slip and sliding process is induced by applying the oblique or transverse load is also considered. The account for memory effects in the slip regime and for configurational effects in the sliding regime is essential in the analysis.

2. The sphere-sphere contact interaction for the displacement controlled sliding process

Two cases of the sphere-sphere contact interaction under the imposed trajectory will be considered (Fig. 1).

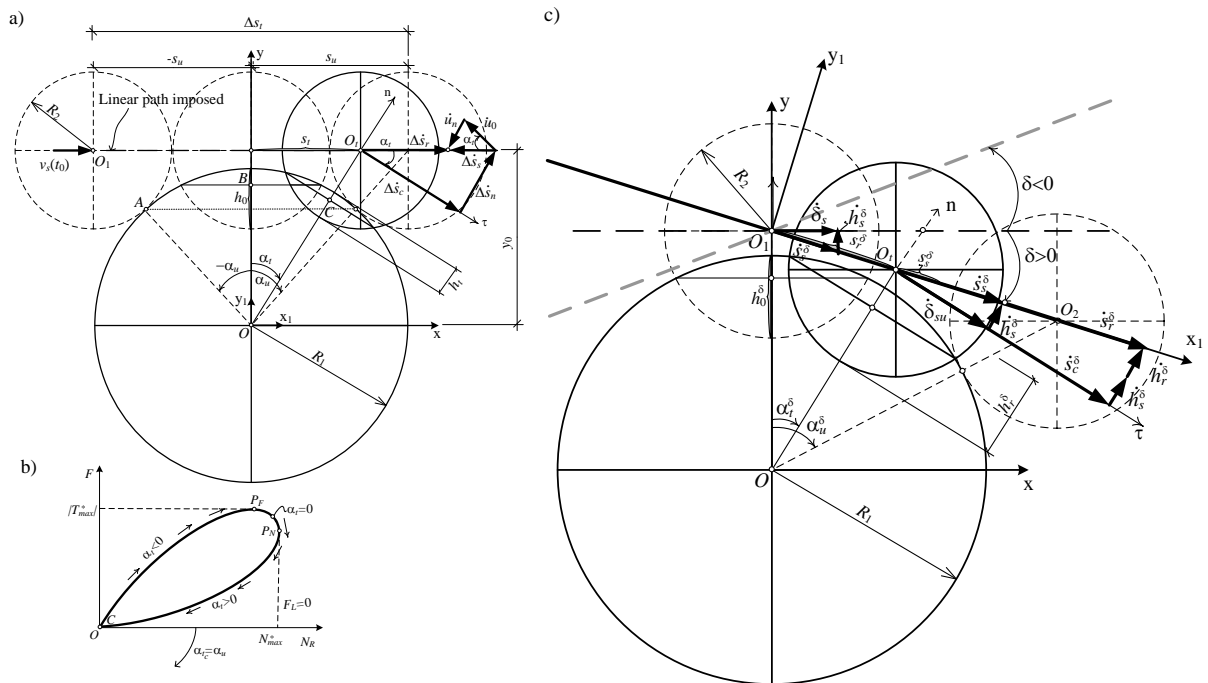


Fig. 1. Sphere-sphere contact interaction - geometry and decomposition of velocities: a) horizontal sphere centre trajectory inducing contact engagement in the combined slip-sliding mode, b) inclined linear motion trajectory applied after initial contact generation by normal loading.

Firstly, we shall consider the sliding of the sphere of radius R_2 along the imposed linear path O_1O_2 (Fig. 1a). In this case, the sphere comes into contact at the point A and translates over the lower sphere until the contact separation. Next, the analysis of the sphere slip and sliding will be performed for the motion along an inclined trajectory relative to the activated contact zone by the primarily normal compression introduced, (Fig. 1b). The displacement controlled process is executed by mounting the upper sphere at the center point O_1 to a moving tool which imposes the required motion trajectories and eliminates the sphere rotation.

The contact modelling is performed using the normal contact traction specified by the Hertz law $N(h_t) = k_n^* h_t^{3/2}$ (where h_t is the total overlap defined as the sum of penetration depths of the contacting spheres, $k_n^* = 4/3 E_{eff} \sqrt{R_{eff}}$ is the contact zone stiffness depending on the effective modulus of elasticity E_{eff} and the effective radius R_{eff} of two contacting spheres) and adopting the tangential contact traction accounting for the Mindlin-Deresiewicz and Coulomb sliding friction rules.

The contact path is specified geometrically by tracking the contact point C position during sliding by intersection of sphere profiles (cf., Fig. 1a). Since the Hertz theory defines the normal contact force N between two spheres of different elastic compliance and radii in terms of total overlap h_t , so there is no need to select a specific contact trajectory for each case of different elastic compliances and radii. The mechanical contact response depends on the evolution of total overlap and of the orientation of contact plane. In Fig. 1a, the contact point position C shown is attributed to the actual path for the spheres of equal elastic moduli.

2.1. Contact zone activated in the sliding mode interacting with slip displacement

Consider the sliding of sphere of radius R_2 along the linear path O_1O_2 (Fig. 1a). The contact condition is $R - y_0 > 0$ (where $R = R_1 + R_2$, y_0 is the vertical coordinate of the sphere center), while the value of maximal overlap h_0 is known. Hence, the condition of $y_0 = R - h_0 = const$ is held. The contact zone growth develops instantaneously in the sliding mode and the Coulomb friction rule is valid from the onset of contact engagement [4], when the following initial condition is satisfied

$$y_0 \geq y_{lim} = \frac{(2-\nu)\mu}{4(1-\nu)} R, \tag{1}$$

where μ is the coefficient of friction and ν is the Poisson's ratio.

However, a *limit* slip displacement δ_u , tangential to the contact plane, specified in Mindlin-Deresiewicz theory [1], develops simultaneously with the sliding displacement Δs_r at the sphere centre and evolves along the whole sliding path. Therefore the slip and sliding rates are interacting and, therefore, affecting the overlap. Thus, we can assume (Fig. 1a):

$$\Delta \dot{s}_t = \Delta \dot{s}_s + \Delta \dot{s}_r, \quad \dot{h}_t = \dot{h}_s + \dot{h}_r \tag{2}$$

where Δs_s is the slip displacement component related to the limit displacement δ_u and \dot{h}_s, \dot{h}_r are the corresponding overlap rates. Note, the slip displacement is referred to the sphere center tangential to the contact plane, but the contact zone position at point C remains fixed.

The ultimate slip displacement and its rate, for the left- or rightward motions, can be expressed as:

$$u_0 = s_g \delta_u = s_g (2 + \nu) \mu h_t / 4 = \chi h_t, \quad \dot{u}_0 = \chi \dot{h}_t, \tag{3}$$

where $\chi = s_g (2 + \nu)\mu/4$ and $\dot{h}_t = \dot{h}_s + \dot{h}_r$ are the normal contact velocities of the contact plane produced by slip and sliding displacements Δs_s and Δs_r , respectively, $s_g = \text{sign}(v_s(t_0))$ is the function setting the direction of motion.

From the contact configuration developed at angle α_t , the following relations can also be written (Fig. 1a)

$$\Delta \dot{s}_r = y_0 \dot{\alpha}_t / \cos^2 \alpha_t ; \quad \Delta \dot{s}_s = \dot{u}_0 / \cos \alpha_t = \chi (\dot{h}_s + \dot{h}_r) / \cos \alpha_t , \quad (4)$$

where $\dot{h}_r = -y_0 \dot{\alpha}_t \sin \alpha_t / \cos^2 \alpha_t$, $\dot{h}_s = -\dot{u}_0 \tan \alpha_t$ and $\dot{u}_0 = \chi \dot{h}_r / (1 + \chi \tan \alpha_t) = -\chi \Delta \dot{s}_r \tan \alpha_t / (1 + \chi \tan \alpha_t)$.

Thus, the sphere centre translation and the total overlap rates are expressed as follows:

$$\Delta \dot{s}_t = \Delta \dot{s}_r + \Delta \dot{s}_s = \Delta \dot{s}_r / (1 + \chi \tan \alpha_t) \approx (1 - \chi \tan \alpha_t) \Delta \dot{s}_r , \quad (5)$$

$$\dot{h}_t = \dot{h}_r + \dot{h}_s = \dot{h}_r / (1 + \chi \tan \alpha_t) \approx (1 - \chi \tan \alpha_t) \dot{h}_r , \quad (6)$$

while the functions of the sphere displacement, center coordinate and overlap are found after integration. Thus:

$$\Delta s_t(\alpha_t) \approx y_0 \left[(\tan \alpha_t - \tan \alpha_0) - (\chi/2) (\tan^2 \alpha_t - \tan^2 \alpha_0) \right], \quad s_t(\alpha_t) \approx y_0 \left[(\tan \alpha_t) - (\chi/2) (\tan^2 \alpha_t - \tan^2 \alpha_0) \right] \quad (7)$$

$$h_t(\alpha_t) \approx y_0 / (2 \cos \alpha) (\chi (\tan \alpha - \cos \alpha \ln((1 + \sin \alpha) / \cos \alpha)) - 2) \Big|_{\pm \alpha_u}^{\alpha_t} . \quad (8)$$

where α_0 is the initial angle of contact engagement: $\alpha_0 = -\alpha_u$, for $s_g = 1$, and $\alpha_0 = \alpha_u$ for $s_g = -1$. Note that for $h_t(\alpha_t) = 0$, the contact separation angle α_u is specified.

The imposed trajectory induces the contact forces, while the equilibrium conditions express the resultant forces oriented in the normal and parallel directions to the translation path imposed:

$$N^*(\alpha_t) = N(\alpha_t) \cos(\alpha_t - s_g \phi) / \cos \phi, \quad N_R = N^* , \quad (9)$$

$$T^*(\alpha_t) = N(\alpha_t) \sin(\alpha_t - s_g \phi) / \cos \phi, \quad F = -T^* , \quad (10)$$

where $\phi = \arctan \mu$ is the friction angle, N_R is the vertical reaction force of the moving tool and F is the moving tool driving force.

Now, the active loading condition, accounting for the contact plane orientation can be expressed by the formula

$$F_L(N_R, F, \alpha_t) = T^*(\alpha_t) - N^*(\alpha_t) \tan(\alpha_t - s_g \phi) = F(\alpha_t) + N_R(\alpha_t) \tan(\alpha_t - s_g \phi) = 0 . \quad (11)$$

In Fig. 1b, the force function $F-N_R$ for the case of monotonic rightward motion along the linear trajectory and evolution of the limit surface (11), represented by two Coulomb lines rotating about the origin O , is plotted. During sliding the limit locus rotates, as the angle α_t varies from $-\alpha_u$ to α_u from the contact activation to its separation, respectively. The force path reaches the maximal value of the driving force F at point P_F , for $\alpha_T \leq 0$. Next, the extremal point P_N is attained at $\alpha_N \geq 0$ at which vertical reaction takes the maximal value. Thus, the combined slip and sliding memory rules are represented by the N_R-F limit and loading surfaces with account for the contact plane rotation an any α_t .

The contact orientations corresponding to maximal values of T_{\max}^* and N_{\max}^* can be determined from the formulae (9)-(10), requiring $dT^*/d\alpha_i = 0$ and $dN^*/d\alpha_i = 0$, and the following equations are derived:

$$\tan \alpha_T = 2/3(\cos \alpha_T / \cos \alpha_u - 1) \cot(\alpha_T - s_g \phi), \tag{12}$$

$$\tan \alpha_N = -2/3(\cos \alpha_N / \cos \alpha_u - 1) \tan(\alpha_N - s_g \phi), \tag{13}$$

where α_T and α_N are the contact angles corresponding to extreme values of resultant forces T^* and N^* .

The derived formulae (12) and (13) can be effectively adopted in the experimental measurement of the coefficient of friction of the spherical grains. In Eq. (12) and (13), the angles α_T , α_N and $\cos \alpha_u = y_0/R$ are the variables independent of the contact stiffness; so, the values of angles α_T (or α_N) can be measured at the peak of the moving tool driving force T_{\max}^* and the friction coefficient can be easily calculated from formulae (12-13).

As a rule, the developed inter-particle friction apparatus [6], [7] are mainly based on the force controlled slip or sliding process. In this case, after contact activation the slip regime evolves first, and next the sphere sliding develops, during which the coefficient of friction is usually predicted. The measurements are very complex because it is difficult to perform exactly initial contact activation due to surface shape imperfections leading the spurious oscillations of the horizontal force. It is worth mentioning that force oscillations tracked during experiment theoretically can be attributed to instantaneous switch from the slip to sliding mode and otherwise. Also, the experimental measurement should be controlled for both vertical loading force and the horizontal driving force.

On the contrary, when the sphere-sphere contact interaction results from the imposed linear motion trajectory, it does not require contact activation by applying the vertical force and generates the sliding mode instantaneously with no preceding slip mode. So, for the experimental prediction of μ , the measurement of angle α_T , at which the driving force magnitude reaches the maximal value, is only required.

2.2. Contact response starting from initially activated contact zone

Consider the case (Fig. 1c), where the sphere motion proceeds from the activated contact at $\alpha_{t0}^\delta = 0$. This is the most frequent case in contact analysis and experimental testing. The initially imposed normal load N_0 activates the contact zone of radius a_0^δ and overlap h_0^δ . The subsequent slip and sliding of the upper sphere relative to a fixed bottom sphere is then induced by the translation paths inclined at the angle δ . When the sphere moves along the inclined trajectory, the contact zone evolves by changing its orientation and size (Fig. 1c).

The main contact parameters, generalized for any case of contact geometry and spheres size, can be defined in the following dimensionless forms: $\bar{s}_r^\delta(\alpha_t^\delta) = \bar{y}_0 \sin \alpha_t^\delta / \cos(\alpha_t^\delta - \delta)$, $\bar{y}_r^\delta(\alpha_t^\delta) = \bar{y}_0 (1 + \tan \delta \tan \alpha_t^\delta)^{-1}$, where $\bar{h}_r^\delta = h_r^\delta / R$, $\bar{y}_r^\delta = y_r^\delta / R$, $\bar{y}_0 = k_r$, $\bar{s}_r^\delta = s_r^\delta / R$.

For the case (Fig. 1c), the resultant forces acting on x_1, y_1 axes, either for the slip or sliding modes, are as follows:

$$N_1^*(\alpha_t^\delta) = N(h_t^\delta) \cos(\alpha_t^\delta - \delta) + s_g [\min(\mu N(h_t^\delta), T(\delta_s))] \sin(\alpha_t^\delta - \delta), \tag{14}$$

$$T_1^*(\alpha_t^\delta) = N(h_t^\delta) \sin(\alpha_t^\delta - \delta) - s_g [\min(\mu N(h_t^\delta), T(\delta_s))] \cos(\alpha_t^\delta - \delta), \tag{15}$$

where $T(\delta_s)$ is the force parallel to the contact plane, induced by the slip displacement δ_s .

After contact activation the imposed translation results in the slip displacement δ_s generated at the sphere center under the fixed contact zone at $\alpha_t^\delta = 0$ (Fig. 1b). The slip regime always proceeds first with displacement δ_s (Fig. 1b), while the normal and tangential displacements are $s_s^\delta = s_t^\delta = \delta_s / c \circ \mathfrak{S}$ and $h_s^\delta = \delta_s \tan \delta$. Moreover, when the sphere motion proceeds from $\alpha_{t0}^\delta = 0$, the sphere center displacement is equal to path coordinate. The overlap takes the additional component $h_t^\delta = h_0^\delta + h_s^\delta$, and the normal contact force now equals:

$$N(h_t^\delta) = k_n^* (h_0^\delta + \delta_s \tan \delta)^{3/2}. \quad (16)$$

At the end of slip regime, when the slip displacement reaches its limit value, $\delta_s = \delta_{su} = \chi h_t^\delta = (N_{su}/k_n^*)^{2/3}$, the switch from the slip to sliding regime occurs and we have:

$$h_{su}^\delta = (N_{su}/k_n^*)^{2/3} = h_0^\delta / (1 - \chi \tan \delta), \quad \delta_{su} = \chi h_0^\delta / (1 - \chi \tan \delta), \quad s_{su}^\delta = \chi h_0^\delta / (1 - \chi \tan \delta) / \cos \delta. \quad (17)$$

$$N_{su} = k_n^* (h_0^\delta)^{3/2} (1 - \chi \tan \delta)^{-3/2}, \quad T(\delta_s) = \mu N_{su} [1 - [1 - \delta_s / \delta_{su}]^{3/2}], \quad \delta_s \in [0, \delta_{su}]. \quad (18)$$

When $\delta_s \geq \delta_{su}$, the sliding regime develops and the sphere slides at varying overlap h_t , contact plane orientation α_t^δ and the limit slip displacement δ_{su} . The trajectory coordinate is $s_t^\delta = s_s^\delta + s_r^\delta$ and the tangential force obeys the Coulomb friction rule, $T(\delta_s) = \mu N(h_t^\delta)$. The problem becomes statically determinate and using Eqs. (14) and (15) we derive the following formula for the driving force:

$$F(\alpha_t^\delta) = -N_1^*(\alpha_t^\delta) \tan(\alpha_t^\delta - \delta - s_g \phi). \quad (19)$$

where $N_1^*(\alpha_t^\delta) = N(h_t^\delta) \cos(\alpha_t^\delta - \delta - s_g \phi) / \cos \phi$ is the resultant force of the moving tool along y_1 -axis.

In the sliding regime, we refer to the velocity decomposition plotted in (Fig. 1b), thus using Eq. (2) $v_s = \dot{s}_t^\delta = \dot{s}_s^\delta + \dot{s}_r^\delta$, where $\dot{s}_s^\delta = \dot{\delta}_{su} / \cos(\alpha_t^\delta - \delta)$, and $\dot{s}_r^\delta = y_0 \cos \delta \dot{\alpha}_t^\delta / \cos^2(\alpha_t^\delta - \delta)$. The limit slip displacement $\delta_{su} = \chi h_t^\delta$, evolves until the contact separation with the rate $\dot{\delta}_{su} = \chi \dot{h}_t^\delta$, while the normal contact velocity is composed of slip and sliding components, $\dot{h}_t^\delta = \dot{h}_s^\delta + \dot{h}_r^\delta$, represented as the overlap rates. Since $\dot{h}_s^\delta = -\dot{\delta}_{su} \tan(\alpha_t^\delta - \delta)$, combining the late three equations we have $\dot{\delta}_{su} = \chi (\dot{h}_r^\delta - \dot{\delta}_{su} \tan(\alpha_t^\delta - \delta))$, which finally yields the following rate equation $\dot{\delta}_{su} = \chi (1 + \chi \tan(\alpha_t^\delta - \delta)) \dot{h}_r^\delta$. The sphere center translation velocity and overlap rate are expressed by the following formulae: $\dot{s}_t^\delta = \dot{s}_s^\delta + \dot{s}_r^\delta \approx (1 - \chi \tan(\alpha_t^\delta - \delta)) \dot{s}_r^\delta$, $\dot{h}_t^\delta = \dot{h}_r^\delta / (1 + \chi \tan(\alpha_t^\delta - \delta))$, $\dot{h}_r^\delta = -y_0 \cos \delta \sin(\alpha_t^\delta - \delta) \dot{\alpha}_t^\delta / \cos^2(\alpha_t^\delta - \delta)$. Finally, integration of these equations yields:

$$s_t^\delta(\alpha_t^\delta) \approx s_{su}^\delta + y_0 \cos \delta (\tan(\alpha - \delta) - \chi \cos^{-2}(\alpha - \delta) / 2) \Big|_0^{\alpha_t^\delta}, \quad (20)$$

$$h_t(\alpha_t) \approx h_{su} + y_0 \cos \delta / (2 \cos(\alpha - \delta)) [\chi (\tan(\alpha - \delta) - \ln((1 + \sin(\alpha - \delta)) / \cos(\alpha - \delta)) \cos(\alpha - \delta)) - 2] \Big|_0^{\alpha_t^\delta}. \quad (21)$$

In Fig. 2a, the driving force-path diagrams are plotted for the different radii of the spheres, but the same direction of motion along three trajectory angles equal $\delta = -10^\circ$, $\delta = 0^\circ$ and $\delta = 10^\circ$. The value of $h_0 = 0.01R_1$ was assumed for all sphere sizes and the stiffness modulus was set as $E_{eff} = 1Pa$, yielding $k_n^* = 4/3 \sqrt{R_{eff}}$.

a)

b)

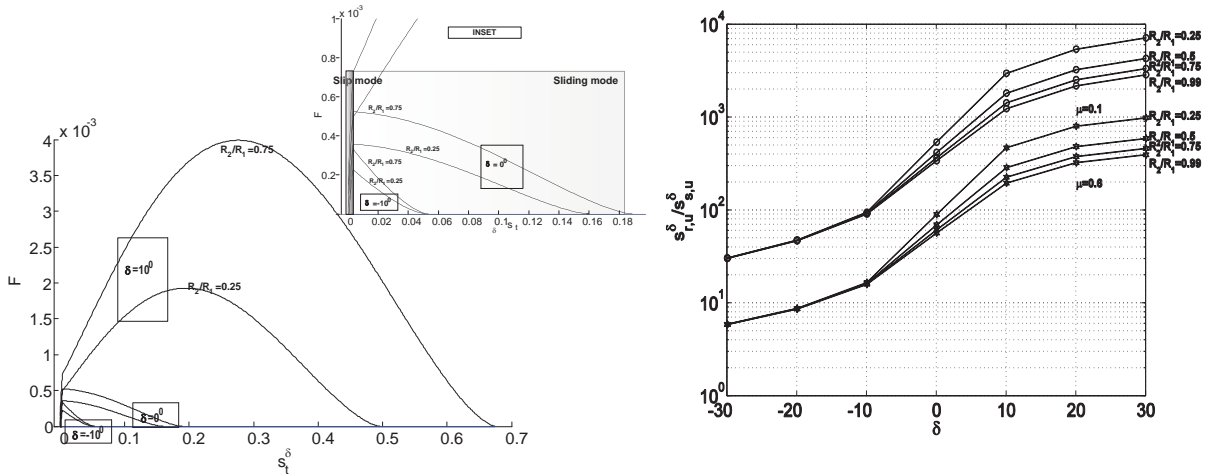


Fig. 2. Combined slip-sliding modes under the inclined paths imposed: a) driving force-path diagrams for the imposed trajectory angles: $\delta > 0$, $\delta = 0$, $\delta < 0$, b) sliding to slip displacement ratio limits vs. the coefficient of friction, sphere radii and trajectory inclination angle.

The driving force-path diagrams indicate different deformation processes after contact activation (Fig. 2a). In particular, for the case $\delta > 0$ (*uploaded sliding*) the maximal driving force values are up to 4 times higher than in case of *transverse sliding*, $\delta = 0$, and even more higher relative the case of *unloaded sliding*, $\delta < 0$, where the normal force unloading takes place during the whole imposed sliding path. In the total displacement scale, the driving force values evolve almost instantaneously in the slip mode (Fig. 2a, inset), and next during the sliding mode the force evolution strongly depends on the contact plane rotation with respect to the trajectory inclination.

It is seen that different maximal values of the driving force can be reached at different stages of sphere motion with consecutive slip and sliding regimes. For $\delta < 0$, the maximal driving force is reached in the slip mode with transition to sliding mode at the reduced force value. For $\delta = 0$ the transverse slip mode passes to sliding mode at the maximal force value. When $\delta > 0$, the maximal value of driving force is reached in the sliding mode, i.e., the driving force-path diagram is initially related to continuous increase of the overlap h_t^δ for all contact plane configuration angles, such that $\alpha_t^\delta < \delta$. On the other hand, for contact plane configurations corresponding to $\alpha_t^\delta > \delta$, the continuous decrease of driving force magnitude occurs in the sliding mode up to contact separation. It is important to note that, when the driving force amplitude is increased during experimental cyclic loading, then near the driving force peak value the small contact surface imperfection of grain can lead a spurious jump from the slip displacement to excessive sphere sliding with the subsequent effect of ratcheting. This effect has been observed in some cyclic loading tests of contact response, cf [7].

The dependence of ratio limits for sliding to slip displacement on coefficient of friction, sphere radii ratio and trajectory inclination angles is diagrammatically presented in Fig. 2b. It can be seen that the inequality $s_{sl}^\delta \ll s_{ru}^\delta$ is valid; however, for $\delta < 0$, the limit slip displacement s_{sl}^δ is about 3.3 times smaller than the sliding limit displacement s_{ru}^δ . The effect of slip displacement should then be accounted for in the contact response analysis, especially, for cyclic loading programs.

3. Conclusions

For the combined slip and sliding regimes, a brief set of relations specifying the sphere motion under the displacement controlled processes has been presented. The account for the *memory effects* in the slip regime and the *configurational effects* in the sliding regime is essential in the analysis. Further applications and extensions of the analysis can be envisaged in the development of the translation controlled apparatus for the measurement of friction and restitution coefficients for the pair of spherical grains. The translation controlled apparatus could be simpler in application and *advantageous* in measurement than the load controlled apparatus. Also, the analysis presented is

suitable for characterization of the aggregate production processes and in the analysis of wear problems along with the specification of the flash temperature effect in the contact zone of two spherical grains.

References

- [1] P.A. Cundall, O.D.L. Strack, A discrete numerical model for granular assemblies, *Geotechnique* 29 (1979) 47–65
- [2] R. Balevičius, I. Sielamowicz, Z. Mróz, R. Kačianauskas, Effect of rolling friction on wall pressure, discharge velocity and outflow of granular material from a flat-bottomed bin, *Particuology* 10 (2012) 672–682.
- [3] R.D. Mindlin, H. Deresiewicz, Elastic spheres in contact under varying oblique forces, *Journal of Applied Mechanics* 20 (1953) 327–344.
- [4] R. Balevičius, Z. Mróz, A finite sliding model of two identical spheres under displacement and force control - part I: static analysis, *Acta Mechanica* 224(8) (2013) 1659–1684.
- [5] R. Balevičius, Z. Mróz, A finite sliding model of two identical spheres under displacement and force control. Part II: dynamic analysis. *Acta Mechanica* 225 (2014) 1735–1759.
- [6] J. Łukaszuk, M. Molenda, J. Horabik, J. Wiącek, Method of measurement of coefficient of friction between pairs of metallic and organic objects, *Acta Agrophysica* 13(2) (2009) 407–418 (in Polish).
- [7] D.M. Cole, Laboratory observations of frictional sliding of individual contacts in geologic materials, *Granular Matter* 17 (2015) 95–110.